International Journal of Nanomedicine

Dovepress
open access to scientific and medical research

Open Access Full Text Article

ORIGINAL RESEARCH

Plasmonic MXene-based nanocomposites exhibiting photothermal therapeutic effects with lower acute toxicity than pure MXene

This article was published in the following Dove Press journal:
International Journal of Nanomedicine

Essraa A Hussein[1]
Moustafa M Zagho[1]
Balsam R Rizeq[2,3]
Nadin N Younes[4]
Gianfranco Pintus[3,4]
Khaled A Mahmoud[5]
Gheyath K Nasrallah[3,4]
Ahmed A Elzatahry[1]

[1]Materials Science and Technology Program, College of Arts and Sciences, Qatar University, Doha, Qatar; [2]Department of Biological and Environmental Sciences, College of Arts and Sciences, Qatar University, Doha, Qatar; [3]Biomedical Research Center, Qatar University, Doha, Qatar; [4]Department of Biomedical Science, College of Health Sciences, Qatar University, Women's Science Building, Doha, Qatar; [5]Qatar Environment and Energy Research Institute (QEERI), Hamad Bin Khalifa University, Doha, Qatar

Correspondence: Gheyath K Nasrallah
Department of Biomedical Science, College of Health Sciences, Qatar University, Women's Science building, C01, P.O Box: 2713, Doha, Qatar
Tel +9 744 403 4817
Fax +9 744 403 1351
Email gheyath.nasrallah@qu.edu.qa

Ahmed A Elzatahry
Materials Science and Technology Program, College of Arts and Sciences, Qatar University, PO Box 2713, Doha, Qatar
Tel +9 744 403 4817
Fax +9 743 387 2847
Email aelzatahry@qu.edu.qa

Purpose: Here, we fabricated two plasmonic 2D $Ti_3C_2T_x$-based nanocomposites (Au/MXene and Au/Fe_3O_4/MXene) with similarly high anti-cancer photothermal therapy (PTT) capabilities, but with less in vivo toxicity than a pure MXene.

Methods: Au/MXene was synthesized by in situ reduction of tetrachloroauric acid using $NaBH_4$ on $Ti_3C_2T_x$ flakes. For targeted PTT, magnetic Au/Fe_3O_4/MXene was synthesized via a reaction between freshly prepared magnetite Fe_3O_4 NPs and MXene solution, followed by in situ integration of gold nanoparticles (AuNPs).

Results: Morphological characterization by XRD, SEM, and TEM revealed the successful synthesis of Au/MXene and Au/Fe_3O_4/MXene. Both new composites exhibited a significant in vitro dose-dependent PTT effect against human breast cancer cells MCF7. Interestingly, in vivo acute toxicity assays using zebrafish embryos indicated that Au/MXene and Au/Fe_3O_4/MXene had less embryonic mortality ($LC_{50} \gg 1000$ µg/mL) than pure MXene (LC_{50}=257.46 µg/mL).

Conclusion: Our new Au/MXene and Au/Fe_3O_4/MXene nanocomposites could be safer and more suitable than the pure MXene for biomedical applications, especially when targeted PTT is warranted.

Keywords: MXene, gold, magnetite, MCF7, photothermal therapy, acute toxicity

Introduction

With the promising evolution of nanotechnology, nano-scaled materials have been devoted to a wide range of applications including magnetics, photonics, catalysis, medicines, cosmetics, and pharmaceutics.[1–4] Since the discovery of graphene, scientists have been paid special attention for two-dimensional (2D) nanomaterials owing to their intriguing physiochemical characteristics and ultrathin morphology.[5–7] Therefore, recent studies focusing on 2D inorganic compounds as graphene analogs have extended in recent years.[8,9] MXene, a new class of outstanding 2D materials including transition metal carbides or carbonitrides with several novel properties, has been synthesized by Gogotsi, Barsoum, and colleague.[10–14] MXenes can be synthesized by etching the A-element from the highly stacked MAX phases, in which M is an early transition metal such as Titanium (Ti), A is an A-group element, and X can be either C or N. Based on its ultrathin structure, MXene offers superior characteristics such as hydrophilic surface and outstanding physicochemical performance when compared to other 2D materials.[5–7] MXenes were explored in many promising applications such as ion sieving[15] as well as energy conversions and storage.[16–20] In the biomedical field,

$Ti_3C_2T_x$ MXenes have been employed for several applications such as antibacterial,[21] biosensors,[22] and photothermal therapy.[23] Moreover, MXene quantum dots have been prepared as biocompatible cellular imaging probe due to their extra small size and luminescence properties.[24] It is noteworthy to mention that a unique photothermal agent based on ultrathin $Ti_3C_2T_x$ MXene nanosheets displayed remarkable in vivo photothermal ablation of tumor cells using a mouse model in vivo.[25]

Photothermal therapy (PTT) is considered as a noninvasive cancer therapy in which tumor cells killing is achieved using the heat produced upon nanocomposites exposure to the near-infrared radiation (NIR).[26–28] Light energy absorption by the PTT induces an electron excitation status inside the PTT agent atoms, which is followed by nonradiative energy relaxation. This process leads to a kinetic energy gaining, which results in the production of heat within the environment around the PTT agents.[29–31] Heat-associated thermal energy induces the damage of several cell structural components including proteins and membranes eventually lead to the death of cells within the tumor area.[32] In this context, because of their unique optical properties, noble metals such as gold (Au) and silver (Ag) exhibit a well-known photo-physical phenomenon called localized surface plasmon resonance, which contributes to enhancing their intrinsic photo-absorption characteristics.[33–36] For this reason, they can be functionalized as image-guided photothermal cancer therapy[37,38] or PTT agents due to their propensity to generate hyperthermia in tumor cells when irradiated with a laser light.[39–41] Akin to Au- and Ag-structured nanoparticles, $Ti_3C_2T_x$ (MXene) nanocomposites, having transition metal element (titanium), exhibit a strong NIR absorption as well as subsequent light-to-heat conversion property resulting in photon-induced hyperthermia. Indeed, the exfoliated ultrathin MXene nanosheets, like other transition metal dichalcogenides such as titanium sulfide (TiS_2), tungsten sulfide (WS_2), and molybdenum sulfide (MoS_2),[42,43] exhibit semimetal-like band energy structure, and so, they offer the local surface plasmon resonance effect and counted as promising PTT agents similar to metal nanoparticles.[25]

Although both MXenes and Au nanostructures are recognized as powerful PTT agents,[23] they can be further engineered by the addition of magnetite iron oxide nanoparticles (Fe_3O_4 NPs) to act as magnetic carriers directed to a specific target by the effect of a magnetic field.[44] In this work, two $Ti_3C_2T_x$ (MXene)-based nanocomposites (Au/MXene and Au/Fe_3O_4/MXene) have been chemically synthesized to investigate their potential application as photothermal therapy agents after the integration of Au and Fe_3O_4 NPs to $Ti_3C_2T_x$ nanosheets. In particular, the integration of magnetite Fe_3O_4 NPs was applied to add the advantage of a tumor-targeted therapy and thus avoid drugs leakage to the normal tissues. In addition, as a further step toward the potential in vivo application of our newly synthesized compounds, we also evidenced their safety using the zebrafish embryo as an in vivo experimental model.

In this report, we investigated the photothermal ablation activity of Au/MXene and Au/Fe_3O_4/MXene as two novel MXene-based nanocomposites on the human cancer cell line (MCF7) and correlated between their photothermal activities and in vivo toxicity (using the zebrafish model), compared to the pure $Ti_3C_2T_x$ MXene. Our two MXene-based nanocomposites demonstrated a reasonable in vitro PTT against the human breast cancer cells MCF7 and showed less in vivo toxicity than the pure MXene, indicating that our new MXene-based nanocomposites could be safer and more suitable than the pure Mxene for PTT applications.

Materials and methods

Chemicals

Aluminum titanium carbide powder (Ti_3AlC_2, or MAX phase) was purchased from Carbon-Ukraine ltd. Hydrofluoric acid (HF, 48%) was supplied by Merck Schuchardt OHG, Germany. Dimethyl sulfoxide (DMSO) was obtained from Honeywell Riedel-de Haën®, Germany. For Fe_3O_4 synthesis, $FeCl_3$ powder, trisodium citrate, and ethylene glycol were purchased from Fisher Scientific, Waltham, USA. Sodium acetate was from Breckland Scientific Supplies, Stafford, United Kingdom. Ethanol absolute was supplied by Sisco Research Laboratories, Mumbai, India. The $AuCl_4$ powder was purchased from Sigma-Aldrich, and $NaBH_4$ fine granular solid was provided by Merck Schuchardt OHG, Germany for Au nanoparticles preparation. For the toxicity study, zebrafish (*Danio rerio*) embryos (AB) strains were used. 4-N,N-diethylaminobenzaldehyde (DEAB) was purchased from Sigma-Aldrich and used as a positive control in the acute toxicity assay. DEAB is an aldehyde dehydrogenase isoenzymes inhibitor that causes teratogenic and toxic effects. The E3 medium used for growth and nutrition was composed of sodium chloride, potassium chloride, magnesium sulfate heptahydrate, and calcium chloride

dihydrate. Addition of phenylthiourea (PTU) to E3 media was utilized as a negative control. PTU was used to inhibit the formation of melanin in zebrafish embryos, which makes the embryos appear transparent, and thus easier for imaging. The 1X PTU working solution was prepared by adding 13.2 mL of egg water to 13.2 mL of PTU (60X) and add 40 µL of methylene blue and fill it to 1000 mL of water. For the in vitro photothermal tumor ablation studies, human breast cancer cells (MCF7) were purchased from American Type Culture Collection ATCC, Manassas, VA, USA. DMEM (Gibco® Laboratories, Thermo Fisher Scientific, USA) supplied with 10% FBS and 1% P/S (penicillin and streptomycin) was used to maintain the cells in a humidified incubator at 37°C and 5% CO_2. Almar blue cell viability reagent (Invitrogen, Thermo Fisher Scientific) was used to assess cell viability following the kit protocol. Water was purified using a Milli Q system (Millipore, Molsheim, France).

Characterization and measurements

The morphology of the synthesized materials was investigated using X-ray diffraction (XRD), scanning electron microscope (SEM), transmission electron microscope (TEM), dynamic light scattering (DLS), and vibrating sample magnetometer (VSM) measurements. PAN analytical X-Ray diffractometer was equipped at room temperature to carry out XRD analysis of the prepared materials. This technique was operated with a Cu-Kα1 radiation source (λ=1.5405 Å), employing Bragg–Brentano geometry. It was performed at 45 KV, and 20 mA, and the results were obtained in a 2θ range from 2° to 50°, with a step size of 0.013°. NOVA NANOSEM 450 (N-SEM) was employed to study the composites morphology with a voltage of 500 V to 30 KV. Talos Transmission Electron Microscope (FEI) was used for TEM, operated at 200 KV and provided with a new Ceta 16 M camera that zooms from a large field of view to atomic scale. The as-prepared nanocomposites were sonicated for 2 hrs, and one drop of each solution was dispersed on a carbon-coated grid. After solvent evaporation, samples were processed in TEM. Microtrac NANOTRAC WAVE II particle size zeta potential analyzer was used for characterization of our materials to detect the size distribution as well as the aggregation pattern. About 6 DLS measurements were achieved, and the average size distribution was recorded. To study the magnetic properties of the prepared Fe_3O_4 NPs and Au/Fe_3O_4/MXene nanocomposite, DynaCool PPMS with the Vibrating Sample Magnetometer attachment was used in our experiment. DanioScope is a noninvasive video analysis tool used to investigate several parameters in zebrafish larvae such as chorion activity and morphology. This DanioScope was supplied from Noldus Information Technology Company. The source of NIR radiation was an 808 nm high power multimode pump laser (Shanghai Connet Fiber Optics Company), operated at different power density from 0 to 2 W cm^{-2}. Vernier Go!Temp (Beaverton, Oregon, USA), a temperature probe, was used to measure the temperature of solutions upon irradiation with an 808-nm laser. Spectrophotometer (ELISA Reader, Epoch 2 Microplate Reader, Bio-Tek, US) was utilized to evaluate cell viabilities.

Synthesis of MXene-based nanocomposites

Synthesis of $Ti_3C_2T_x$ (MXene)

$Ti_3C_2T_x$ (MXene) was prepared by etching of MAX phase using HF as previously described by Naguib et al[12]. About 50 mL concentrated HF (48%) was added to 5 g Ti_3AlC_2 powder and stirred for 18 hrs at room temperature. After that, the reaction solution of etched MAX was diluted with 100 mL deionized water and centrifuged for 10 mins. The sediment was washed several times with deionized water until the pH of the supernatant is 5. The etched MAX is intercalated with DMSO for 24 hr and then delaminated by ultra-sonication under argon gas. The resulted solution was then centrifuged for 1 hr at 4°C to obtain the desired delaminated MXene solution.

Synthesis of magnetite (Fe_3O_4) nanoparticles

The magnetite Fe_3O_4 nanoparticles were synthesized according to the referenced solve-thermal method.[45] Ferric chloride ($FeCl_3$) powder was subjected to a reduction reaction by the effect of ethylene glycol in the presence of trisodium citrate and sodium acetate. The resultant solution was inserted in stainless steel autoclave at 200°C for 10 hrs. Then, the precipitate of Fe_3O_4 nanoparticles was washed, sonicated, and collected by a strong magnet.

Preparation of Fe_3O_4/MXene nanocomposite

MXene aqueous solution was mixed with the as-prepared magnetite Fe_3O_4 nanoparticles suspension in a ratio of 5:1 by weight, respectively. The mixture was ultra-sonicated for 2 hrs. Afterwards, centrifugation for 20 mins was employed, and the obtained supernatant was collected for characterization.

In situ preparation of Au/MXene and Au/Fe_3O_4 /MXene nanocomposites

The deposition of Au nanoparticles on MXene or Fe_3O_4 /MXene wad done following the procedure mentioned by

Qi et al with modification.[46] Briefly, 50 mg of $AuCl_4$ was dissolved in 1 mL of deionized water followed by 50× dilution. The diluted solution was then added to either MXene or Fe_3O_4/MXene and sonicated for 2 hrs. Then, 1 mL of freshly prepared 1 M $NaBH_4$ solution was added to the two sonicated mixtures, stirred overnight, and centrifuged for the preparation of (Au/MXene) and (Au/Fe_3O_4/MXene) nanocomposites, respectively. Finally, the precipitate was washed twice by high-speed centrifugation and collected.

Acute toxicity studies using zebrafish embryos

All zebrafish experiments were accomplished in accordance to national and international guidelines for the use of zebrafish in experimental settings and according to the animal protocol guidelines required by the Department of Research in the Ministry of Public Health, Qatar.[47] About 150 embryos were taken to 12-well plates with 25 embryos per well. The first 6 wells were filled with 3 mL of PTU (served as negative controls) while the other wells were filled with different concentrations of DEAB (0.1, 1, 10, 100 µM, and 1 mM; served as positive controls), all dissolved with PTU to a total volume of 3 mL per well. After that, 200 embryos were transferred to another 12-well plate with 25 embryos in each well (8 wells) for treatment with different concentrations (0, 50, 100, and 200 µg/mL) of each nanocomposite (Au/MXene and Au/Fe_3O_4/MXene). The two 12-well plates were then covered and left in the incubator for 24–96 hpf. The embryos were observed under the ZEISS SteREO Lumar.V12 microscope at 48, 72, and 96 hpf for any teratogenic effect including mortality, body deformity, escoliosis, pigmentation, yolk edema, heart edema, and movement defects. The photographs for teratogenic effects or embryos malformation were captured, and the results were recorded. More details about this part are included in Supplementary material.

In vitro photothermal tumor ablation examinations

Cell culture

A confluent cell culture flask of human breast cancer cells (MCF7) was washed with PBS (pH=7.4) followed by trypsinization using 0.05% Trypsin-EDTA (1× solution). The single cell suspension was counted and seeded in 96-well culture plates with a final concentration of 1×10^4 cells/well in the supplemented DMEM. The cells were incubated and allowed to adhere overnight at 37°C and 5% CO_2.

Incubation of MCF7 cells with the as-prepared nanocomposites

The complete growth media of MCF7 seeded cells were changed the next day with fresh culture medium containing Au/MXene, Au/Fe_3O_4/MXene composites (separately) with different concentrations (0, 50, 100, 200, and 400 µg/mL). The same procedure was followed with MXene material alone with concentrations of (0, 50, 100, and 200 µg/mL).

Laser exposure and measurement of the percentage of cell viability

After 24 hrs of incubation, the cells were irradiated for 5 mins using 808-nm high power multimode pump laser (Shanghai Connet Fiber Optics Company) at different output power densities (0, 0.3, 0.5, 1.0, and 1.5 W cm^{-2}). Finally, Alamar Blue reagent was added (10 µL/100 µL culture media in each well) and the plates were incubated at 37°C for 4 hrs. To evaluate cell viability, reading was performed using microplate reader at an excitation wavelength of 570 nm as previously described.[48] The results were expressed as the mean of cell viability percentage and normalized to the control (no laser-treated cells). Three replicates were done for each treatment group.

Statistical analysis

Chi–square test was applied to calculate the significance between the percentages for the hatching rate. For the rest of the experiment, data were expressed as mean ± SD or SE, and statistical evaluation of significance was performed by one-way ANOVA and Tukey's test. Significant differences were calculated at (*)=$p<0.05$; (**)=$p<0.01$; (***)=$p<0.001$.

Results

Morphological and dispersion properties of MXene-based nanocomposites

XRD analysis was employed for MXene in addition to the fabricated Fe_3O_4 NPs+ and the nanocomposites (Au/MXene and Au/Fe_3O_4/MXene) as shown in Figure 1. Additionally, SEM images of MXene, Fe_3O_4 NPs, the prepared hybrid of Fe_3O_4/MXene, as well as the two composites are illustrated in Supporting Information, Figures S1–S3.

TEM was used for characterization of Au/MXene and Au/Fe_3O_4/MXene composites to investigate the presence of the attached nanoparticles on MXene surface. TEM images of the samples are presented in Figures 2A and B. The

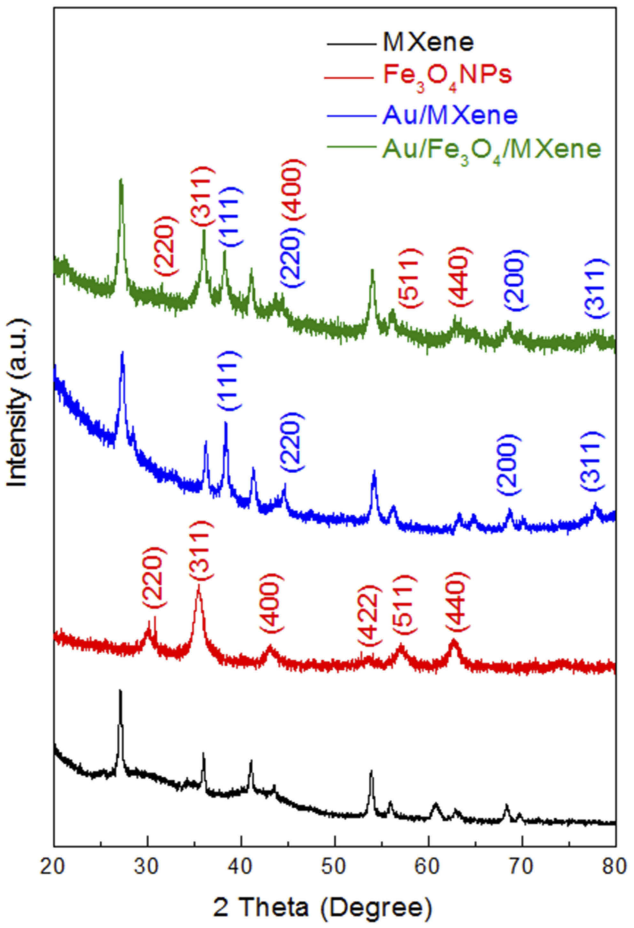

Figure 1 XRD pattern for MXene, Fe_3O_4 NPs, Au/MXene, and Au/Fe_3O_4/MXene.

diameters of both Au and Fe_3O_4 NPs showed that loaded particles are in the nano size (from 5 nm or less up to 10 nm).

DLS was performed to detect the size distribution of pure MXene and the two prepared composites (Supporting Information, Figure S4). VSM was applied to demonstrate the magnetization of ferromagnetic materials such as the prepared Fe_3O_4 NPs and Au/Fe_3O_4/MXene composite under the effect of the applied magnetic field, as shown in Figure S5, Supporting Information.

Embryonic acute toxicity and teratogenicity analysis

Acute toxicity assays were performed to investigate the toxicity of the as-prepared Au/MXene and Au/Fe_3O_4 /MXene nanocomposites on survival and early developmental stages of zebrafish. In general, using living organisms in the early stages is favorable for investigating acute toxicity due to their higher sensitivity to toxicological agents, which means a more reliable determination of lethal and sublethal effects.[49,50] Zebrafish embryos were exposed to three different concentrations (50, 100, and 200 µg/mL) of Au/MXene and Au/Fe_3O_4/MXene from 24 to 96 hpf. Figure 3 represents the acute toxicity and teratogenicity analysis results measured at 96 hpf. Figure 3A demonstrates the normal development of the Au/MXene and Au/Fe_3O_4/MXene-treated embryo groups when compared to the DEAB-treated positive (exhibited severe malformation and teratogenic effects). By using GraphPad Software, the LC_{50} value for DEAB was calculated to be 2.564 µM as shown in Figure 3B. For DEAB, the no observed effect concentration (NOEC) scored below 20% at 1.0 µM for the mortality, while the low observed effect concentration (LOEC) scored >30% at 10.0 µM for the teratogenic effect. The teratogenic phenotype analysis revealed that the Au/MXene and Au/Fe_3O_4/MXene manifested almost no acute toxic or teratogenic effect on zebrafish embryos at all tested concentrations (Figure 3C). Both composites have no teratogenic (Figure 3C) or mortality (Figure 3D) effects when compared to DEAB, which caused abnormal development, pigmentation defects, yolk sac edema, heart edema, and motility problems. For this reason, the NOEC, LOEC, and LC_{50} were insignificant and consequently cannot be calculated with the concentrations used in this study.

In vitro photothermal tumor ablation studies

The photothermal performances of three prepared solutions of MXene, Au/MXene, and Au/Fe_3O_4/MXene (200 µg/mL) were investigated via exposure of each solution to an 808 laser (power density=1.0 W/cm^2) for 5 mins. As shown in Figure S6, the temperature exhibited a gradual increase to around 43.0°C and 39.3°C in the case of Au/MXene and Au/Fe_3O_4/MXene, respectively. On the other hand, it was noticed that the temperature elevation in pure MXene solution recorded higher temperature (≈46.8°C), exceeding those of Au/MXene and Au/Fe_3O_4/MXene nanocomposites.

The photothermal conversion ability of Au/MXene and Au/Fe_3O_4/MXene was evaluated at the cell level using MCF7 breast cancer cell line (human breast adenocarcinoma cell line). After incubation with different concentrations of both nanocomposites (0, 50, 100, and 200 µg/mL) for 24 hrs, the cell viability was measured using Alamar Blue cell viability reagent. Relative cell viability was assessed with and without laser exposure. No obvious cytotoxicity was observed in the case of "No Laser"

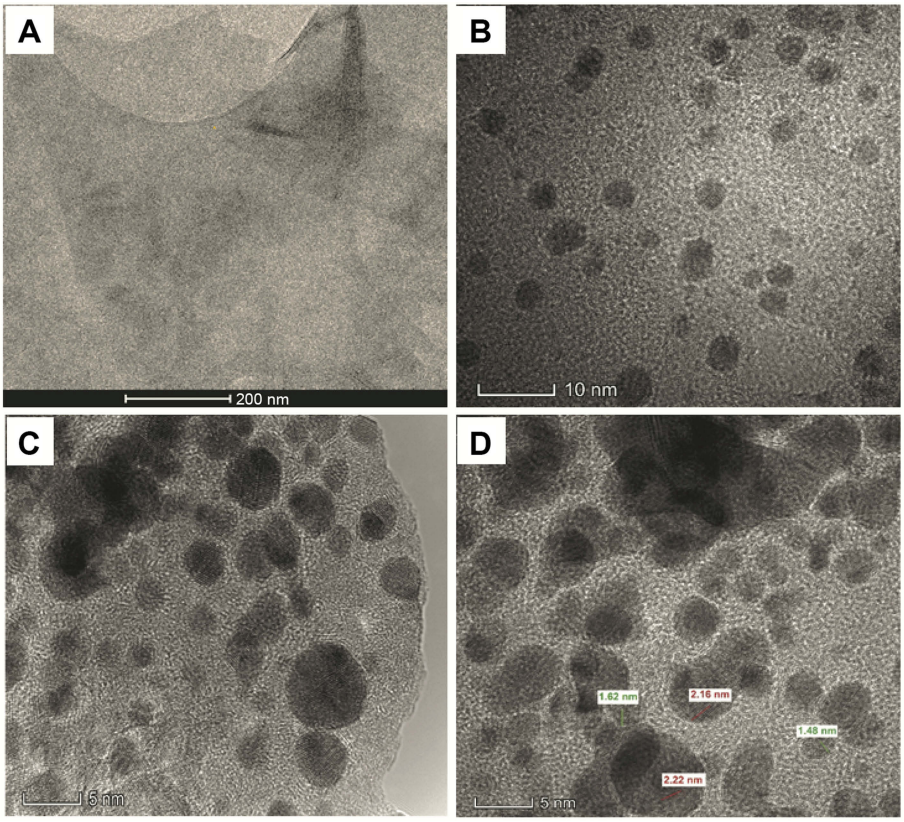

Figure 2 (**A**) TEM image for pure MXene, (**B**) TEM image for Au/MXene composite showing AuNPs on the surface of MXene sheets, (**C**) TEM image for Au/Fe_3O_4/MXene composite showing AuNPs and Fe_3O_4 NPs on MXene surface, (**D**) high-resolution TEM image for Au/Fe_3O_4/MXene nanocomposite showing two types of nanoparticles (Au and Fe_3O_4) with two different d-spacing values.
Abbreviations: AuNPs, gold nanoparticles; TEM, transmission electron microscopy.

even at a high concentration indicating the high biocompatibility of both composites (Figure 4). To estimate the photothermal conversion (ablations) performance, the two nanocomposites were exposed to an 808-nm NIR laser (1.0 W/cm^2). In the case of laser exposure for 5 mins, cell viability decreased gradually with increasing concentrations of Au/MXene and Au/Fe_3O_4/MXene (Figure 4). Next, we wanted to test whether tumor ablation ability of Au/MXene and Au/Fe_3O_4/MXene increases by increasing the power density of the laser diode. Therefore, photothermal therapeutic efficiency was investigated by the exposure one concentration of both nanocomposites (200 µg/mL) to 808-nm laser operated at various power densities (0.0, 0.3, 0.5, 1.0, and 1.5 W/cm^2). As shown in Figure 5, the ablation performance augmented in a dose-dependent manner with an increasing laser power intensity.

Discussion

The overall synthesis of the two nanocomposites of (Au/MXene) and (Au/Fe_3O_4/MXene) was accomplished as previously mentioned.[12,45] For the fabricated nanocomposites, XRD was used to confirm the presence of Au NPs in Au/MXene composite and both AuNPs and Fe_3O_4NPs in Au/Fe_3O_4/MXene composite (Figure 1). The four characteristic peaks for Au NPs were observed in the two composite samples and can be ascribed to the (111), (200), (220), and (311) reflection planes of cubic structure of gold NPs and the obtained results were compared with the reference standard powder diffraction file of ICSD:52700, ICDD:00–004-0784, and ICDD:98–005-2700 which proves that particles obtained are gold nanoparticles.[51] The observed six diffraction peaks for magnetite Fe_3O_4 in the 2θ range 20–80° could be described as the (220), (311), (400), (422), (511), and (440) reaction planes of the monoclinic structure of magnetite (Fe_3O_4).[45,52]

Preparation of MXene nanoflakes was employed via etching of Ti_3AlC_2 (MAX phase), intercalation with DMSO, and delamination of the intercalated MXene solution. By comparison, SEM images imply the difference between the solid compact MAX powder and the loosely packed structure, which is the etched MAX (Supporting

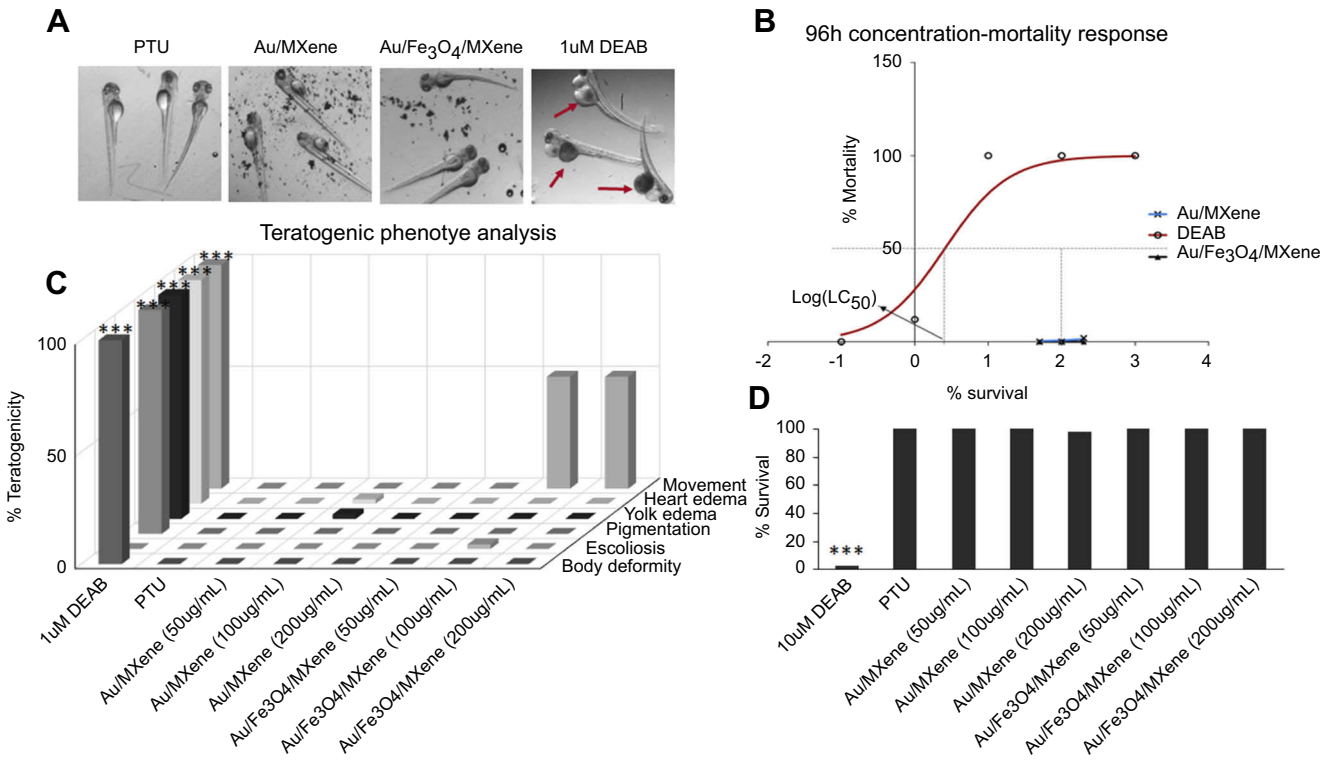

Figure 3 Acute toxicity and teratogenicity analysis for Au/MXene and Au/Fe_3O_4/MXene using DEAB as a positive control and PTU as a negative control. (**A**) Acute toxicity pictures were taken at 96 hpf using stereomicroscope. (**B**) Cumulative mortality and LC_{50} calculation using GraphPad Software. (**C**) Teratogenic phenotype analysis at different concentrations of the synthesized nanocomposites. (**D**) Percentage survival curve after treatment with different contents of DEAB, Au/MXene, and Au/Fe_3O_4 /MXene. Percent survival was calculated at 96 hpf. Significant differences were calculated at (***) = p <0.001.

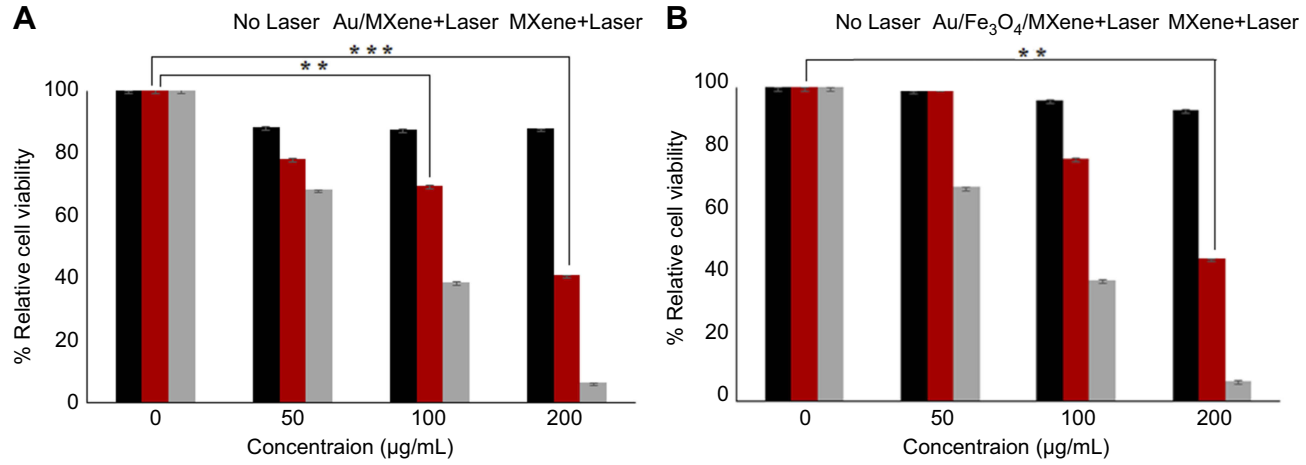

Figure 4 Relative viabilities of MCF7 cells after incubation with different concentrations of (**A**) Au/MXene and b) Au/Fe_3O_4/MXene, and MXene followed by NIR 808-nm laser irradiation at the power density of 1.0 W/cm^2 for 5 mins. Data are represented as the mean ± SE for triplicates and normalized to the control (no laser-treated cells). The experiments were done in three different times, and similar results were obtained. Significant differences were calculated at (**)=p<0.01; (***)=p<0.001.

Information, Figure S1). The magnetite Fe_3O_4 nanoparticles were synthesized according to the referenced solvothermal method.[45] The as-prepared particles have a spherical shape and a nearly uniform size (Supporting Information, Figure S2). TEM images showed a uniform distribution of the nanoparticles as well as a coating of a large portion of $Ti_3C_2T_x$ surface. To differentiate between Au and Fe_3O_4 NPs in the hybrid Au/Fe_3O_4/MXene composite, high-resolution TEM was conducted to determine the d-spacing for each particle (Figures 2C and D). Two different values were obtained and compared with the reference values for d-spacing of Au NPs and magnetite Fe_3O_4 NPs. In agreement

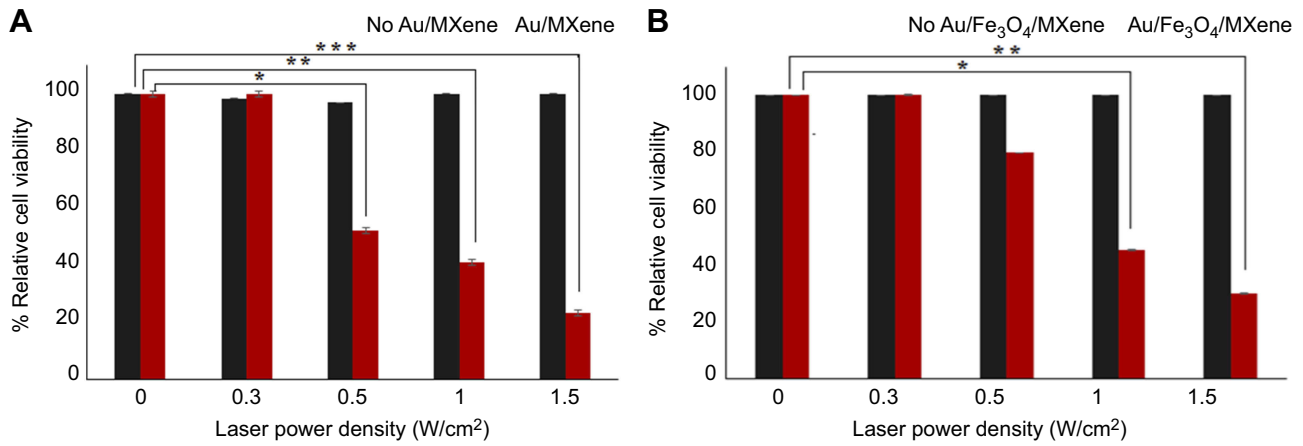

Figure 5 Relative viabilities of MCF7 cells after incubation with (**A**) Au/MXene and (**B**) Au/Fe_3O_4/MXene, and exposure to NIR 808-nm laser at different laser power densities for 5 mins. Data are represented as the mean ± SE for triplicates and normalized to the control (no laser-treated cells). The experiments were done in three different times, and similar results were obtained. Significant differences were calculated at (*)=p<0.05; (**)=p<0.01; (***)=p<0.001.

with references, the d-spacing of the most intense diffraction peak (111) for Au NPs equals 1.62 Å[51] while that of (311) peak for Fe_3O_4 NPs equals 2.5 Å according to the standard powder diffraction reference of ICSD:164814 and ICDD: 98–016-4814 for magnetite Fe_3O_4.

Generally, our initial findings of the embryonic toxicity revealed there were no significant developmental toxicity or lethal effects when zebrafish embryos were exposed to the as-prepared (Au/MXene) and (Au/Fe_3O_4 /MXene) nanocomposites. To explain, Au nanoparticles (present in both mixtures) were proven to be more biocompatible and less toxic when compared to other nanoparticles such as Ag or Pt.[53,54] The reasonable explanation that was reported by Browning et al[55] attributed this observation to the random Brownian diffusion of Au nanoparticles inside the embryo, which in turn resulted in the random accumulation of the nanoparticles in different parts. Consequently, this different distribution with various Au nanoparticles amount ended up to less alteration of embryonic morphology, development, and life span. The magnetite Fe_3O_4 nanoparticles are widely used because they can be easily functionalized besides their beneficial properties such as hydrophilicity, stability in aqueous suspensions, as well as their ability to bind to bioactive molecules.[56] The reported mechanism for the potential impact of iron NPs is due to aggregation and sedimentation phenomenon, which means that the NPs will tend to agglomerate and settle down into the medium. As the zebrafish embryos are benthic organisms, the NPs sedimentation allows the direct contact between them. That is why the zebrafish embryos are a good model for assessment of iron NPs toxicity. Zhu et al[57] revealed that nano-Fe_2O_3 delayed the hatching rate and caused developmental abnormalities, heart edema, and even mortality in some embryos. On the contrary, Piccinetti et al[56] found that there was no tissue damage, and no significant effect on the survival rate and when compared the Fe_3O_4 NPs-treated embryos to the untreated control group. To our knowledge, this is the first study for assessment of Fe_3O_4 NPs when mixed with other nanomaterials. Our results showed that the mixture containing Fe_3O_4 NPs did not exhibit significant teratogenicity or lethal effects. One replicate group only showed some movement problems as presented in Figure 3.

Assessment of the potential toxicity is considered as a critical point when comparing our findings of acute toxicity study of both Au/MXene and Au/Fe_3O_4/MXene composites with the recently published toxicity study of pure MXene using the same model[58] which manifested that MXene has some teratogenic and toxicological effects starting from concentration of 100 µg/mL. The authors reported that the LOEC for MXene was at 100 µg/mL (with cumulative mortality at ≈21%). Moreover, the hypothetical LC_{50} should of our nanocomposites should be ≫ 1000 µg/mL while that of pure MXene, which was calculated in the same published study,[58] was expected to be of 257.46 µg/mL, suggesting that Au/MXene and Au/Fe_3O_4/MXene could be used as a surrogate for Mxene when PTT or any another in vivo biomedical application is needed. These findings are considered the evidence for the relative biocompatibility and safety of

Au/MXene and Au/Fe_3O_4/MXene when compared to pure MXene.

Dose-dependent responses, as well as power density-dependent responses, were investigated. As shown in Figures 4 and 5, the tumor ablation ability increases by increasing either the concentrations of the nanocomposites or the power density of the laser diode, respectively. The highest power density (1.5 W/cm^2) caused the best cell killing due to enhanced photothermal activity and temperature increase. Both Au/MXene and Au/Fe_3O_4/MXene exhibited efficient cell killing as they act as PTT agents.

Compared to pure MXene, Au/MXene and Au/Fe_3O_4/MXene nanocomposites showed reduced photothermal activity (Figure 4). The possible chemical explanation could be due to the integration of nanoparticles during reaction with MXene, which affect the nanostructure of ultrathin MXene sheets.[59] This effect was illustrated in our DLS results that showed an increase in the size distribution and higher aggregation after the integration of NPs to MXene. This size effect would influence the photothermal ability of the nanocomposites compared to MXene. However, the photothermal effect of both nanocomposites is still acceptable as PTT agents for cancer treatment in vitro. Additionally, the integration of magnetite Fe_3O_4 NPs in the Au/Fe_3O_4 /MXene nanocomposite adds an advantage as the magnetite Fe_3O_4 NPs are considered magnetic carriers that could be directed to a specific location in the body using the applied magnetic field as previously illustrated in magnetic hysteresis loop in the VSM test (Figure S5).[60]

According to nano-toxicology basis,[61,62] the addition of nanoparticles to MXene nanosheets might have changes directly related to the potential toxic effects. For instance, the integration of both Au NPs and Fe_3O_4 NPs could affect the ultrathin structure of MXene resulting in an alteration of $Ti_3C_2T_x$ size and stacking of some layers. The resultant changes cause a relative increase in the size and consequently, less toxic effects. Second, it is observed from TEM images that surface of MXene are almost entirely coated with NPs, which means masking of surface charge and functional groups on the surface leading to lower toxicity (Figure 2). Surface charge plays an essential role in nanomaterials toxicity as it can affect the adsorption of ions and biomolecules. Furthermore, modifying the surface charge or surface composition might influence the intracellular distribution and reduce reactive oxygen species production that causes further toxicity. Consequently, the undesired effects of nanomaterials could be mitigated by the incorporation of surface coatings.[61] Compared to recently reported PTT nanoagents for tumor ablation which used the same cell model (MCF7), as presented in Table S1, Au/MXene and Au/Fe_3O_4/MXene show acceptable cell killing in vitro along with high biocompatibility. To sum up, the as-prepared MXene-based nanocomposites are more suitable for in vivo application even at high concentration while MXene is restricted to specific concentration (100 μg/mL).

Conclusion

In conclusion, this study aims to fabricate two novel MXene-based nanocomposites for biomedical application. Designed composites (Au/MXene and Au/Fe_3O_4/MXene) were prepared, characterized, and tested for potential toxic effects on zebrafish embryos. Additionally, their photothermal activities were investigated. The toxicity results revealed no overall embryonic toxicity or teratogenicity effects for the nanocomposites even at high concentrations. Compared to the recently published toxicity study of MXene using zebrafish embryos, the reported Mxene toxicity study showed that MXene caused 21% mortality at a concentration of 100 μg/mL. Therefore, these nanocomposites are considered as practically harmless and surrogate materials for pure MXene. For cancer therapy, our findings were statistically approved and revealed efficient cell killing and photothermal activity for Au/MXene and Au/Fe_3O_4/MXene nanocomposites. Although MXene induced higher photothermal ability, high concentrations of both nanocomposites are less toxic than MXene according to the toxicity study results, which means they are more suitable nanomaterials for biomedical applications. These bio-applied nanomaterials are usually a balance between toxicity and biocompatibility.

Acknowledgments

This work was supported by Qatar University under High Impact-Fund Program Grant QUHI-CAS-19/20-1. The authors are thankful to S. Suslov, A. Samara at the Core lab of QEERI/HBKU, Doha, Qatar, for TEM, DLS, and VSM analysis. The publication of this article was funded by the Qatar National Library. The authors have neither other relevant affiliations nor financial involvement with any entity or organization with a financial conflict with the subject matter or materials discussed in the manuscript apart from those disclosed.

Disclosure

The authors report no conflicts of interest in this work.

References

1. Donaldson K. Resolving the nanoparticles paradox. *Nanomed (Lond)*. 2006;1(2):229–234. doi:10.2217/17435889.1.2.229
2. Kagan VE, Bayir H, Shvedova AA. Nanomedicine and nanotoxicology: two sides of the same coin. *Nanomedicine*. 2005;1(4):313–316. doi:10.1016/j.nano.2005.10.003
3. Linkov I, Satterstrom FK, Corey LM. Nanotoxicology and nanomedicine: making hard decisions. *Nanomedicine*. 2008;4(2):167–171. doi:10.1016/j.nano.2008.01.001
4. Medina C, Santos-Martinez MJ, Radomski A, Corrigan OI, Radomski MW. Nanoparticles: pharmacological and toxicological significance. *Br J Pharmacol*. 2007;150(5):552–558. doi:10.1038/sj.bjp.0707130
5. Novoselov KS, Jiang D, Schedin F, et al. Two-dimensional atomic crystals. *Proc Natl Acad Sci U S A*. 2005;102(30):10451–10453. doi:10.1073/pnas.0502848102
6. Geim AK, Novoselov KS. The rise of graphene. *Nat Mater*. 2007;6:183–191. doi:10.1038/nmat1849
7. Li X, Wang X, Zhang L, Lee S, Dai H. Chemically derived, ultrasmooth graphene nanoribbon semiconductors. *Science*. 2008;319(5867):1229–1232. doi:10.1126/science.1150878
8. Sun Y, Gao S, Lei F, Xiao C, Xie Y. Ultrathin two-dimensional inorganic materials : new opportunities for solid state nanochemistry published as part of the accounts of chemical Research special issue " 2D nanomaterials beyond graphene ". *Acc Chem Res*. 2014;48(1):3–12. doi:10.1021/ar500164g
9. Chen Y, Tan C, Zhang H, Wang L. Two-dimensional graphene analogues for biomedical applications. *Chem Soc Rev*. 2015;44(9):2681–2701. doi:10.1039/C4CS00300D
10. Ghidiu M, Lukatskaya MR, Zhao M-Q, Gogotsi Y, Barsoum MW. Conductive two-dimensional titanium carbide 'clay' with high volumetric capacitance. *Nature*. 2014;516:78–81. doi:10.1038/nature13970
11. Mashtalir O, Naguib M, Mochalin VN, et al. Intercalation and delamination of layered carbides and carbonitrides. *Nat Commun*. 2013;4:1716. doi:10.1038/ncomms2664
12. Naguib M, Kurtoglu M, Presser V, et al. Two-dimensional nanocrystals produced by exfoliation of Ti 3AlC 2. *Adv Mater*. 2011;23(37):4248–4253. doi:10.1002/adma.201102306
13. Naguib M, Gogotsi Y. Synthesis of two-dimensional materials by selective extraction. *Acc Chem Res*. 2015;48(1):128–135. doi:10.1021/ar500346b
14. Naguib M, Mashtalir O, Carle J, et al. Two-dimensional transition metal carbides. *ACS Nano*. 2012;6(2):1322–1331. doi:10.1021/nn204153h
15. Peng Q, Guo J, Zhang Q, et al. Unique lead adsorption behavior of activated hydroxyl group in two-dimensional titanium carbide. *J Am Chem Soc*. 2014;136(11):4113–4116. doi:10.1021/ja500506k
16. Ling Z, Ren CE, Zhao M-Q, et al. Flexible and conductive MXene films and nanocomposites with high capacitance. *Proc Natl Acad Sci*. 2014;111(47):16676–16681. doi:10.1073/pnas.1414215111
17. Lukatskaya MR, Mashtalir O, Ren CE, et al. Cation intercalation and high volumetric capacitance of two-dimensional titanium carbide. *Science*. 2013;341(6153):1502–1505. doi:10.1126/science.1241488
18. Wang X, Kajiyama S, Iinuma H, et al. Pseudocapacitance of MXene nanosheets for high-power sodium-ion hybrid capacitors. *Nat Commun*. 2015;6:6544. doi:10.1038/ncomms7544
19. Xie Y, Dall'Agnese Y, Naguib M, et al. Prediction and characterization of MXene nanosheet anodes for non-lithium-ion batteries. *ACS Nano*. 2014;8(9):9606–9615. doi:10.1021/nn503921j
20. Ren CE, Hatzell KB, Alhabeb M, Ling Z, Mahmoud KA, Gogotsi Y. Charge- and size-selective ion sieving through Ti3C2Tx MXene membranes. *J Phys Chem Lett*. 2015;6(20):4026–4031. doi:10.1021/acs.jpclett.5b01895
21. Rasool K, Helal M, Ali A, Ren CE, Gogotsi Y, Mahmoud KA. Antibacterial activity of Ti3C2Tx MXene. *ACS Nano*. 2016;10(3):3674–3684. doi:10.1021/acsnano.6b00181
22. Xu B, Zhu M, Zhang W, et al. Ultrathin MXene-micropattern-based field-effect transistor for probing neural activity. *Adv Mater*. 2016;28(17):3333–3339. doi:10.1002/adma.201504657
23. Hussein EA, Zagho MM, Nasrallah GK, Elzatahry AA. Recent advances in functional nanostructures as cancer photothermal therapy. *Int J Nanomedicine*. 2018;13:2897–2906. doi:10.2147/IJN.S161031
24. Xue Q, Zhang H, Zhu M, et al. Photoluminescent Ti $_3$ C $_2$ MXene quantum dots for multicolor cellular imaging. *Adv Mater*. 2017;29(15):1604847. doi:10.1002/adma.201604847
25. Lin H, Wang X, Yu L, Chen Y, Shi J. Two-dimensional ultrathin MXene ceramic nanosheets for photothermal conversion. *Nano Lett*. 2017;17(1):384–391. doi:10.1021/acs.nanolett.6b04339
26. Melancon MP, Zhou M, Li C. Cancer theranostics with near-infrared light-activatable multimodal nanoparticles. *Acc Chem Res*. 2011;44(10):947–956. doi:10.1021/ar200022e
27. Kennedy LC, Bickford LR, Lewinski NA, et al. A new era for cancer treatment: gold-nanoparticle-mediated thermal therapies. *Small*. 2011;7(2):169–183. doi:10.1002/smll.201000134
28. Yang K, Feng L, Shi X, Liu Z. Nano-graphene in biomedicine: theranostic applications. *Chem Soc Rev*. 2013;42(2):530–547. doi:10.1039/C2CS35342C
29. Camerin M, Rello S, Villanueva A, et al. Photothermal sensitisation as a novel therapeutic approach for tumours: studies at the cellular and animal level. *Eur J Cancer*. 2005;41(8):1203–1212. doi:10.1016/j.ejca.2005.02.021
30. Camerin M, Rodgers MAJ, Kenney ME, Jori G. Photothermal sensitization: evidence for the lack of oxygen effect on the photosensitizing activity. *Photochem Photobiol Sci*. 2005;4(3):251–253. doi:10.1039/b416418k
31. He X, Bischof JC. Quantification of temperature and injury response in thermal therapy and cryosurgery. *Crit Rev Biomed Eng*. 2003;31(5–6):355–422. doi:10.1615/CritRevBiomedEng.v31.i56.10
32. van der Zee J. Heating the patient: a promising approach? *Ann Oncol*. 2002;13(8):1173–1184. doi:10.1093/annonc/mdf280
33. Dreaden EC, Alkilany AM, Huang X, Murphy CJ, El-Sayed MA. The golden age: gold nanoparticles for biomedicine. *Chem Soc Rev*. 2012;41(7):2740–2779. doi:10.1039/C1CS15237H
34. Dreaden EC, Mackey MA, Huang X, Kang B, El-Sayed MA. Beating cancer in multiple ways using nanogold. *Chem Soc Rev*. 2011;40(7):3391. doi:10.1039/c0cs00180e
35. Huang X, Neretina S, El-Sayed MA. Gold nanorods: from synthesis and properties to biological and biomedical applications. *Adv Mater*. 2009;21(48):4880–4910. doi:10.1002/adma.200802789
36. Lee J, Chatterjee DK, Lee MH, Krishnan S. Gold nanoparticles in breast cancer treatment: promise and potential pitfalls. *Cancer Lett*. 2014;347(1):46–53. doi:10.1016/j.canlet.2014.02.006
37. Chauhan DS, Arunkumar P, Prasad R, et al. Facile synthesis of plasmonic zein nanoshells for imaging-guided photothermal cancer therapy. *Mater Sci Eng C*. 2018;90:539–548. doi:10.1016/j.msec.2018.04.081
38. Chauhan DS, Bukhari AB, Ravichandran G, et al. Enhanced EPR directed and Imaging guided photothermal therapy using vitamin E modified toco-photoxil. *Sci Rep*. 2018;8(1):16673. doi:10.1038/s41598-018-34898-3
39. Jain PK, Huang X, El-Sayed IH, El-Sayed MA. Noble metals on the nanoscale: optical and photothermal properties and some applications in imaging, sensing, biology, and medicine. *Acc Chem Res*. 2008;41(12):1578–1586. doi:10.1021/ar7002804
40. Huang X, Jain PK, El-Sayed IH, El-Sayed MA. Gold nanoparticles: interesting optical properties and recent applications in cancer diagnostics and therapy. *Nanomedicine*. 2007;2(5):681–693. doi:10.2217/17435889.2.5.681

41. Huang X, Jain PK, El-Sayed IH, El-Sayed MA. Plasmonic photothermal therapy (PPTT) using gold nanoparticles. *Lasers Med Sci*. 2008;23(3):217–228. doi:10.1007/s10103-007-0470-x
42. Cheng L, Liu J, Gu X, et al. PEGylated WS2 nanosheets as a multifunctional theranostic agent for in vivo dual-modal CT/photoacoustic imaging guided photothermal therapy. *Adv Mater*. 2014;26(12):1886–1893. doi:10.1002/adma.201304497
43. Zhu Z, Zou Y, Hu W, et al. Near-infrared plasmonic 2D semimetals for applications in communication and biology. *Adv Funct Mater*. 2016;26(11):1793–1802. doi:10.1002/adfm.201504884
44. Basavaiah K, Kahsay MH, RamaDevi D. Green synthesis of magnetite nanoparticles using aqueous pod extract of Dolichos lablab L for an efficient adsorption of crystal violet. *Emergent Mater*. 2018;1(3):121–132. doi:10.1007/s42247-018-0005-1
45. Liu J, Sun Z, Deng Y, et al. Highly water-dispersible biocompatible magnetite particles with low cytotoxicity stabilized by citrate groups. *Angew Chemie - Int Ed*. 2009;48(32):5875–5879. doi:10.1002/anie.200901566
46. Qi P, Chen S, Chen J, Zheng J, Zheng X, Yuan Y. Catalysis and reactivation of ordered mesoporous carbon-supported gold nanoparticles for the base-free oxidation of glucose to gluconic acid. *ACS Catal*. 2015;5(4):2659–2670. doi:10.1021/cs502093b
47. *Ministry of Public Health: Policy on Zebrafish Research*. 2017.
48. Raj MHG, Elmageed ZYA, Zhou J, et al. Synergistic action of dietary phyto-antioxidants on survival and proliferation of ovarian cancer cells. *Gynecol Oncol*. 2008;110(3):432–438. doi:10.1016/j.ygyno.2008.05.001
49. Takeda K, Suzuki K, Ishihara A, et al. Nanoparticles transferred from pregnant mice to their offspring can damage the genital and cranial nerve systems. *J Heal Sci*. 2009;55(1):95–102. doi:10.1248/jhs.55.95
50. Hallare AV, Köhler HR, Triebskorn R. Developmental toxicity and stress protein responses in zebrafish embryos after exposure to diclofenac and its solvent, DMSO. *Chemosphere*. 2004;56(7):659–666. doi:10.1016/j.chemosphere.2004.04.007
51. Al-Hossainy AF, Abd-Elmageed AAI, Ibrahim ATA. Synthesis, structural and optical properties of gold nanoparticle-graphene-selenocysteine composite bismuth ultrathin film electrode and its application to Pb(II) and Cd(II) determination. *Arab J Chem*. 2015. doi:10.1016/j.arabjc.2015.06.020
52. Deng H, Li X, Peng Q, Wang X, Chen J, Li Y. Monodisperse magnetic single-crystal ferrite microspheres. *Angew Chemie Int Ed*. 2005;44(18):2782–2785. doi:10.1002/anie.200462551
53. Lee KJ, Nallathamby PD, Browning LM, Osgood CJ, Xu X-HN. In vivo imaging of transport and biocompatibility of silver nanoparticles in early development of zebrafish embryos. *ACS Nano*. 2007;1(2):133–143. doi:10.1021/nn700048y
54. Asharani PV, Lianwu Y, Gong Z, Valiyaveettil S. Comparison of the toxicity of silver, gold and platinum nanoparticles in developing zebrafish embryos. *Nanotoxicology*. 2011;5(1):43–54. doi:10.3109/17435390.2010.489207
55. Browning LM, Lee KJ, Huang T, Nallathamby PD, Lowman JE, Xu X-HN. Random walk of single gold nanoparticles in zebrafish embryos leading to stochastic toxic effects on embryonic developments. *Nanoscale*. 2009;1:138–152. doi:10.1039/b9nr00053d
56. Piccinetti CC, Montis C, Bonini M, et al. Transfer of silica-coated magnetic (Fe3O4) nanoparticles through food: a molecular and morphological study in zebrafish. *Zebrafish*. 2014;11(6):1–13. doi:10.1089/zeb.2014.1037
57. Zhu X, Tian S, Cai Z. Toxicity assessment of iron oxide nanoparticles in zebrafish (Danio rerio) early life stages. *PLoS One*. 2012;7(9):1–6. doi:10.1371/journal.pone.0046286
58. Nasrallah GK, Al-Asmakh M, Rasool K, Mahmoud KA. Ecotoxicological assessment of $Ti_3C_2T_x$ (MXene) using a zebrafish embryo model. *Environ Sci Nano*. 2018;5(4):1002–1011. doi:10.1039/C7EN01239J
59. Dai C, Lin H, Xu G, Liu Z, Wu R, Chen Y. Biocompatible 2D titanium carbide (MXenes) composite nanosheets for pH-responsive MRI-guided tumor hyperthermia. *Chem Mater*. 2017;29:8637–8652. doi:10.1021/acs.chemmater.7b02441
60. Polyak B, Friedman G. Magnetic targeting for site-specific drug delivery: applications and clinical potential. *Expert Opin Drug Deliv*. 2009;6(1):53–70. doi:10.1517/17425240802662795
61. Sharifi S, Behzadi S, Laurent S, Laird Forrest M, Stroeve P, Mahmoudi M. Toxicity of nanomaterials. *Chem Soc Rev*. 2012;41(6):2323–2343. doi:10.1039/C1CS15188F
62. Rahi A, Sattarahmady N, Heli H. Toxicity of Nanomaterials-Physicochemical Effects. *Austin J Nanomedicine Nanotechnol*. 2014;2:6.